STABILITY ANALYSIS AND CONTROL DESIGN FOR HYBRID AC-DC MORE-ELECTRIC AIRCRAFT POWER SYSTEMS

by

Xiao Li

Submitted to the Graduate Faculty of

Swanson School of Engineering in partial fulfillment

of the requirements for the degree of

Master of Science

University of Pittsburgh

2013

UNIVERSITY OF PITTSBURGH

SWANSON SCHOOL OF ENGINEERING

This thesis was presented

by

Xiao Li

It was defended on

April 1, 2013

and approved by

Zhi-Hong Mao, Ph.D., Associate Professor, Department of Electrical and Computer Engineering

Gregory Reed, Ph.D., Associate Professor, Department of Electrical and Computer Engineering

Thomas McDermott, Ph.D., Assistant Professor, Department of Electrical and Computer Engineering

Thesis Advisor: Zhi-Hong Mao, Ph.D., Associate Professor, Department of Electrical and Computer Engineering

STABILITY ANALYSIS AND CONTROL DESIGN FOR HYBRID AC-DC MORE-ELECTRIC AIRCRAFT POWER SYSTEMS

Xiao Li, M.S.

University of Pittsburgh, 2013

This thesis studies the stability of a more-electric aircraft (MEA) power system with hybrid converters and loads, and proposes a control design method using state feedback. The MEA is aimed to replace the conventional nonelectric power in aircraft with electric power in order to reduce the size and weight of the aircraft power system. This thesis considers a model of the MEA power system consisting of the following components: converters with uncontrolled diodes and controlled rectifiers, ideal constant power loads (CPL), and non-ideal CPL driven by electromechanical actuators. The system has narrow stability range under the conventional two-loop PI control. To improve control performance, a full-state feedback control method is developed that can significantly increase the stability margin of the MEA power system.

TABLE OF CONTENTS

LIST OF TABLES

LIST OF FIGURES

ACKNOWLEDGMENT

At the beginning, I would like to express my sincerely appreciate to my adviser Dr. Zhi-Hong Mao. He always has a way to make me enjoy the research, and give me a strong support on writing this paper. His journal club is excellent and instructive, from which I acquire countless experience.

Secondly, I would like to express my sincerely appreciate to my committee members Dr. Reed and Dr. McDermott for their support on my research. I learned a lot from Dr. Reed last two years. His dedication and concentration affect me a lot.

Thirdly, I have to thank my parents for their great support on both financial and spiritual aspect. Word cannot express my gratitude.

Last but not least, I would like to express my sincerely appreciate to my friends who always encourage me and help me.

1.0 INTRODUCTION

1.1 BACKGROUND

The More-electric aircraft (MEA) concept is presented by military designer in World War II. It underlines to use electric power to replace the conventional power energizing the non-propulsive aircraft system. MEA is a trend for the future development of aircraft.

In a traditional aircraft, fossil energy is mainly converted into propulsive power to move the aircraft. The remainder converted into four parts to power the non-propulsive aircraft system, including hydraulic power, pneumatic power, mechanical power, and electrical power. Hydraulic power, which is transferred from the central hydraulic pump, has to sustain its heavy and inflexible piping, and the serious potential corrosive fluids leakage. Pneumatic power, which is generated from the engines' high pressure compressors, has the disadvantages of low efficiency and difficult leak detection. In addition, each of these four systems has become more and more complex, therefore the connections between them reduce the flexibility and become more difficult. As a consequence, MEA tends to be a solution to reduce the aircraft power systems' size and weight and improve the fuel efficiency. It is believed that to develop an electrical system have far more potential than a conventional one, in order to increase the energy efficiency.

Recently, researches of MEA include two major directions: to increase electrical power generation while reduce the air and hydraulic engines; and to implement electromechanical actuators (EMA) rather than hydraulic actuators. In order to achieve these goals, engineers are searching for highly reliable electrical power systems which using a large amount of power converters. However, not only the development of an efficient and secure power electronic system is a great challenge, but also an efficient control strategy.

In many applications, power electronic technology has the advantage to obtain the best electric power (proper voltage levels and frequencies). Specifically, in a MEA system, the use of converters rather than traditional electromechanical circuit breaker makes the load management and system monitoring simpler and improved flexibility for system upgrades. The converters in an MEA power system are mainly used in two ways: to convert the voltage for buses and to drive the electromechanical actuator. The power electronic based loads in an MEA power system are generally preformed as constant power loads (CPL) when feeding an EMA under current and speed control, which degrade the stability margin of the power system.

Nowadays, worldwide researches of MEA are in progress with different aims. Totally Integrated More Electric Systems (TIMES), aimed to achieve an MEA system using the previously developed system. In order to reduce fuel consumptions as well as the non-propulsive power generation, Power Optimized Aircraft (POA) program devotes to find an optimal method to manage the onboard electrical power on aircrafts, which in the same time increasing the reliability and safety of onboard systems and reducing maintenance costs. In addition, US Air Force MEA Program devoted to providing the military aircraft more electrical capability, etc.[1]

1.2 LITERATURE REVIEW

This chapter reviews some important previous modeling works of power electronics and MEA power systems.

1.2.1 General points

Power electronic loads are generally viewed as the constant power load having small-signal negative impedance which degrades the system stability margin [2][3]. Many literatures studied the model of ideal CPL without dynamics, but few of them consider about the dynamic CPL. In reference [4], it studied controlled electromechanical actuators performed as a CPL having dynamics.

There are three majority methods commonly used for analyzing the performance of power converter systems: state space averaging (SSA) modeling method, average-value modeling (AVM) method, and DQ transformation method. The generalized SSA modeling method, using for analyzing many power converters in DC and AC distribution systems, has represented by [5][6] in DC distribution systems, in the uncontrolled and controlled rectifiers in single-phase [7], and in the 6 and 12 pulse diode rectifiers in three phase ac systems [8]. The AVM method, which has been used for 6 and 12 pulse diode rectifiers, represented in [9]. Another widely used modeling methods for power converters and electromechanical actuator control is the DQ-transformation method [10]. The priority of using DQ transformation method can be seen by comparison with other two methods. The SSA modeling method leads to a complex high-order mathematical model when applied to three-phase AC systems. The AVM method is not easily applicable for vector-controlled converters because it cannot offer the

information on the AC side. The DQ transformation provides lower order system models than SSA and is much easier to apply to a converter controlled in terms of rotation DQ frame aligned with the grid voltage, and represents the converter as a transformer [11],

1.2.2 Generalized aircraft AC electrical power system architecture

Reference [12] presents an aircraft EPS architecture candidate, which is defined in the European MOET project [13], as shown in Figure 1 (see next page). The parameters in this architecture are described in Table 1.

Table 1. The parameters in the MEA architecture

Parameters	Description
R_{eq1}, L_{eq1}, C_{eq1}	the equivalent circuit of the transmission cable linking the generator bus Gen bus and the HVAC bus
R_{TRUj}, L_{TRUj}, C_{TRUj}	AC cable linking HVAC bus and input terminal of the diode rectifier bus
r_{LFj}, L_{Fj}, r_{CFj} and C_{Fj}	DC link filters for diode rectifiers
$P_{idealCPL,De}$	Ideal CPLs (represent other DC loads with regulated DC/DC power converters by assuming an infinitely fast controller action)
$P_{dynCPL,Dn}$	Dynamics of CPL (represent the environmental control system fed through the diode rectifiers)
R_{eq2}, L_{eq2}, C_{eq2}	Transmission line linking the HVAC and the AC essential bus (AC ESS)
R_{conk}, L_{conk}	Input circuit for active PWM controlled rectifiers

Table 1 (continued).

$P_{idealCPL,Pg}$, $P_{dynCPL,Pa}$	The ideal and dynamic CPLs represent other aircraft loads and EMAs (ailerons, rudders, flaps, spoilers, and elevators, etc.)
R_{Lb}, L_{Lb}	The wing de-icing connected to HVAC bus

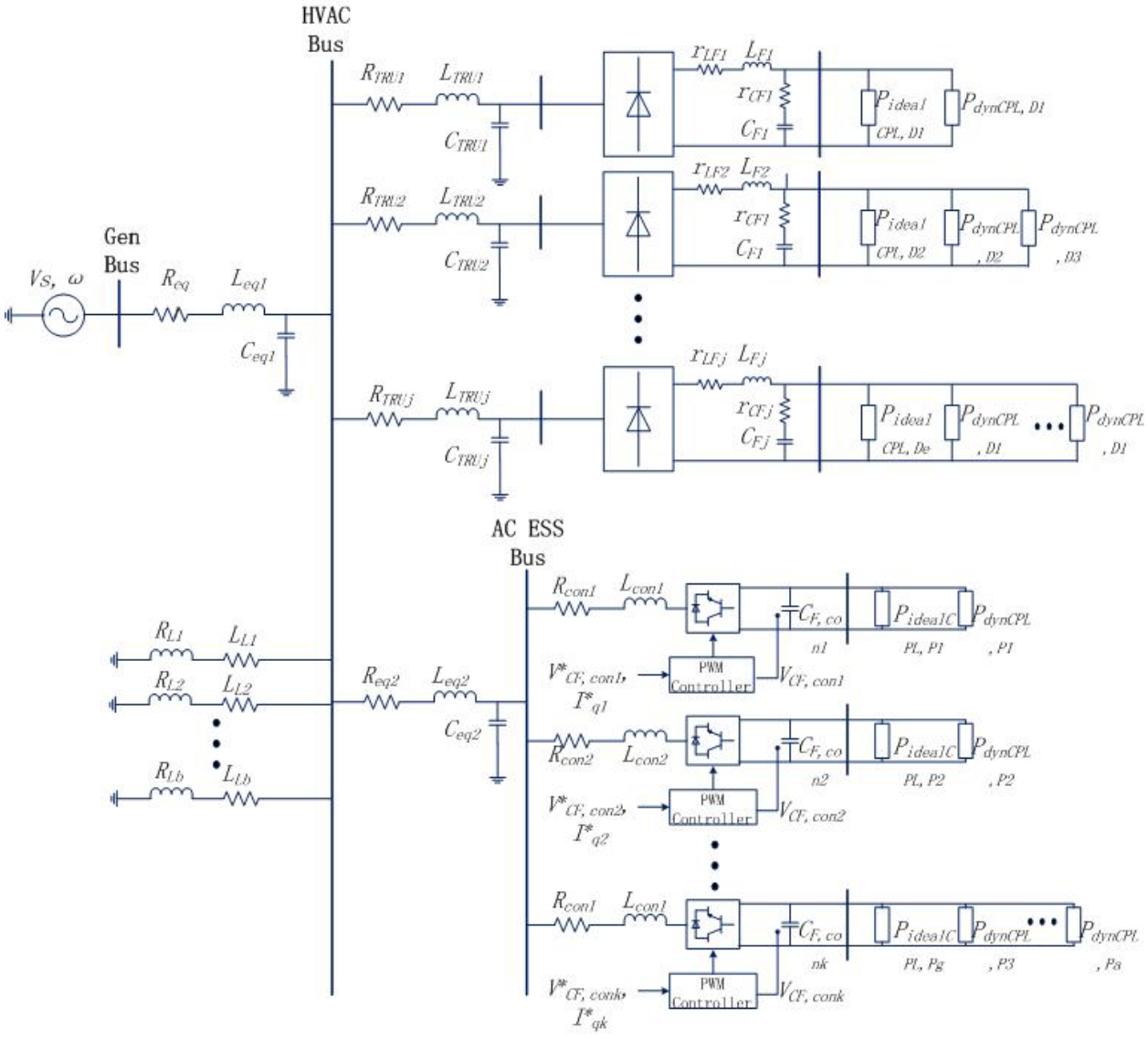

Figure 1. Generalized aircraft AC electrical power system architecture [12]

In this architecture, the diode rectifiers convert the power for the environmental control systems (ECS), which can be viewed as dynamics of CPL $P_{dynCPL,Dn}$, and other DC loads. By assuming an extremely small time constant of controller action, these DC loads can be viewed as ideal CPLs $P_{idealCPL,De}$. The pulse width modulation (PWM) controlled rectifiers feed the other aircraft loads and electromechanical actuators (EMAs) such as elevators, ailerons, rudders, flaps, and spoilers. The model of the controlled PWM rectifier was presented by K-N Areerak in [14].

1.3 THESIS CONTRIBUTION

As we mentioned in the previous section, the prospect of application for MEA are board and many researches have been already in process. However, due to the huge power level requirement in the modern aircraft power system, not only an efficient and secure power electronics technology need to be developed but also a reliable control system of the power electronics.

One of the big challenges for achieving MEA power system is the constant power load (CPL). As we all known, the loads of the power electronic system can be viewed as constant power loads, which significantly degrade the power system stability. A greater power level of MEA system has narrower stability margin which causes the implementation of the MEA impossible at present stage. The widely used control method for improve the system stability is the conventional two-loop PI controller, which typically contains a current control loop as the inner loop and a voltage or power control loop as the outer loop. However, when the two-loop PI controller applies in the MEA system, it only provides a narrow stability margin. In this thesis, a full-state feedback control method is used to enlarge the stability margin, and the result is

verified by MATLAB. Although it is a preliminary and theoretical work, it shows some advantages for using the full-state feedback method to improve the system stability margin.

2.0 METHMETICAL MODEL OF THE MEA POWER SYSTEM

This Chapter presents the derivation of the mathematical model of the studied MEA power system in detail.

2.1 POWER SYSTEM DEFINITIION

The power system studied is shown in Figure 2, which is simplified from the generalized aircraft electrical power system architecture presented in [12]. To reduce the work of the modeling, this thesis uses a controlled rectifier under double loop PI controllers rather than a PWM controller and neglects the parameters of the transmission line between the AC bus and rectifiers. In Figure 2, the controlled rectifier drives an ideal constant load and the uncontrolled diode rectifier drives a PM machine which can be viewed as a dynamic constant load.

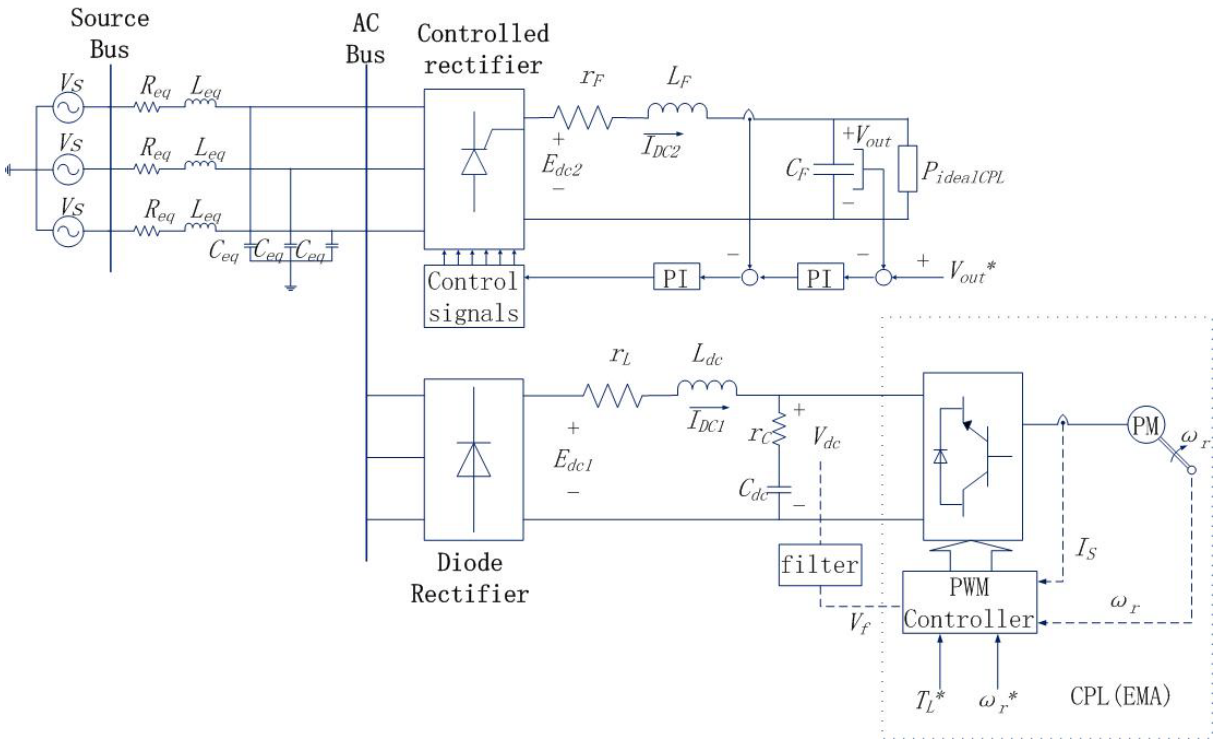

Figure 2. The power system studied

2.2 MODELLING OF SUB-SYSTEMS

In this section, the specified process of the sub-systems modeling will be presented. There are four components in the studied system:

1. Diode rectifier model;

2. Controlled rectifier model;

3. MEA model;

4. Ideal CPL model;

The diode rectifier model and the controlled rectifier model can be constructed as a transformer by applying DQ transformation, which simplifies the analysis process.

2.2.1 Diode rectifier models

At the beginning, let us simply consider about the uncontrolled diode rectifier circuit. To an AC system, the best way to decouple the control of active and reactive power flows is the use of synchronously rotating *d-q* rotating frame [15]. Appling DQ transformation method, the diode rectifier can be modeling as a transformer, which is a convenient and results to a lower order mathematic model. The studied sub-system is shown in the Figure 3.

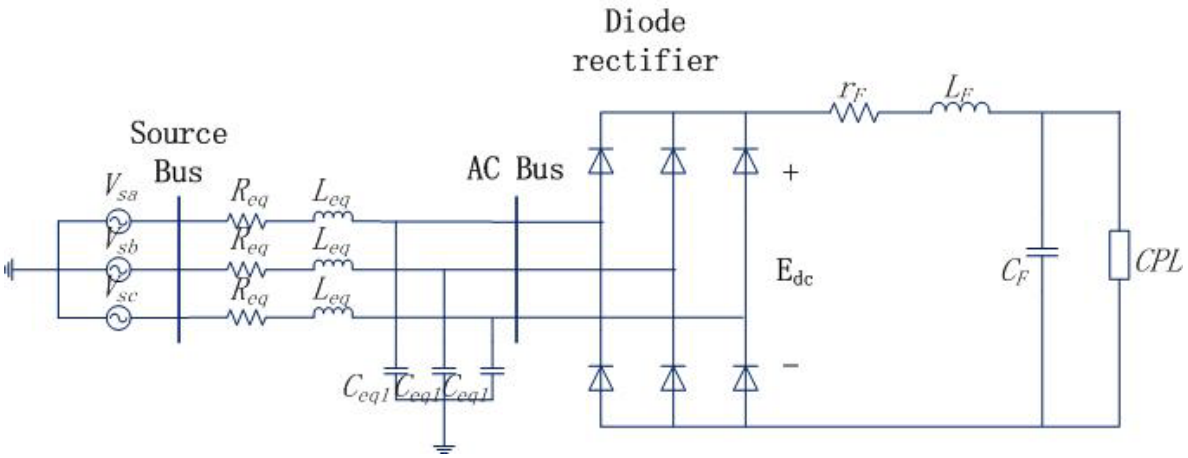

Figure 3. Diode rectifier

2.2.1.1 DQ transformation

The classical DQ transformation process is presented as the following [16]:

If the three phase system is balanced, that is to say,

$$X_a + X_b + X_c = 0 \qquad (2.\ 1)$$

In which vector X_n could be a phase voltage or phase current. Then, we can transfer the reference frame from a stationary three-phase frame to a synchronous rotation *d-q* frame through two steps.

Firstly, applying Clark transformation equation,

$$X_{\alpha\beta} = X_\alpha + jX_\beta = k\left[X_a + X_b e^{-j\frac{2\pi}{3}} + X_c e^{-j\frac{4\pi}{3}}\right] \quad (2.\ 2)$$

Where *k* is a constant number, we achieve the stationary α-β frame. In the matrix form:

$$\begin{bmatrix} X_\alpha \\ X_\beta \end{bmatrix} = k \begin{bmatrix} 1 & -\frac{1}{2} & -\frac{1}{2} \\ 0 & \frac{\sqrt{3}}{2} & -\frac{\sqrt{3}}{2} \end{bmatrix} \begin{bmatrix} X_a \\ X_b \\ X_c \end{bmatrix} \quad (2.\ 3)$$

Secondly, applying Park transformation obtains the rotating *d*-*q* reference frames:

$$\boldsymbol{X_{dq}} = \boldsymbol{X_{\alpha\beta}} e^{-j\theta} \quad (2.\ 4)$$

Now, we have the matrix form transformation equation of transferring directly from abc frame to *d*-*q* frame by substitute (2.3) into (2.4):

$$\begin{bmatrix} X_\alpha \\ X_\beta \end{bmatrix} = k \begin{bmatrix} \cos\theta & \cos(\theta - \frac{2\pi}{3}) & \cos(\theta + \frac{2\pi}{3}) \\ -\sin\theta & -\sin(\theta - \frac{2\pi}{3}) & -\sin(\theta + \frac{2\pi}{3}) \end{bmatrix} \begin{bmatrix} X_a \\ X_b \\ X_c \end{bmatrix} = k\boldsymbol{T} \begin{bmatrix} X_a \\ X_b \\ X_c \end{bmatrix} \quad (2.\ 5)$$

To calculate the vectors in *d*-*q* frame from abc frame, one can simply do the calculation:

$$\boldsymbol{X_{\alpha\beta}} = k^{-1}\boldsymbol{T}^{-1}\boldsymbol{X_{abc}} \quad (2.\ 6)$$

There are two typical value of *k*: $\frac{2}{3}$ and $\sqrt{\frac{2}{3}}$. Each of them has corresponding physical meaning.

If *k* is chosen to be $\sqrt{\frac{2}{3}}$, which is usually called *power invariant*, or *power conserving convention*, this result to the power calculated in the d-q reference frame and the power calculated from abc reference frame will have the same magnitude. If *k* is chosen to be $\frac{2}{3}$, which is usually named as *voltage invariant*, or *peak convention*, this result to the vector quantity in d-q reference frame is equal to the peak of phase quantity in abc reference frame.

The next section shows the process of using DQ transformation method to get the equivalent circuit of the uncontrolled diode rectifier.

2.2.1.2 The equivalent circuit on *d-q* frame

It is best to begin with the analyzing of the rectifier with inductance effect on current commutation. Then the whole equivalent circuit will be easily get by transfer the elements in the abc frame to *d-q* frame.

It is assumed that the converter is operating under the continues-conduction mode and the three phases are balanced. According to Mohan's power electronic text book [17], the inductance L_{eq} in the AC side causes an average DC voltage drop. This is because the inductance current cannot change instantaneous when L_{eq} is finite, which cause an overlap angle during the current commutation process. This voltage drop can be represented as a resistance r_{μ} located on the DC side, depending on the system frequency ω, as shown in Figure 4.

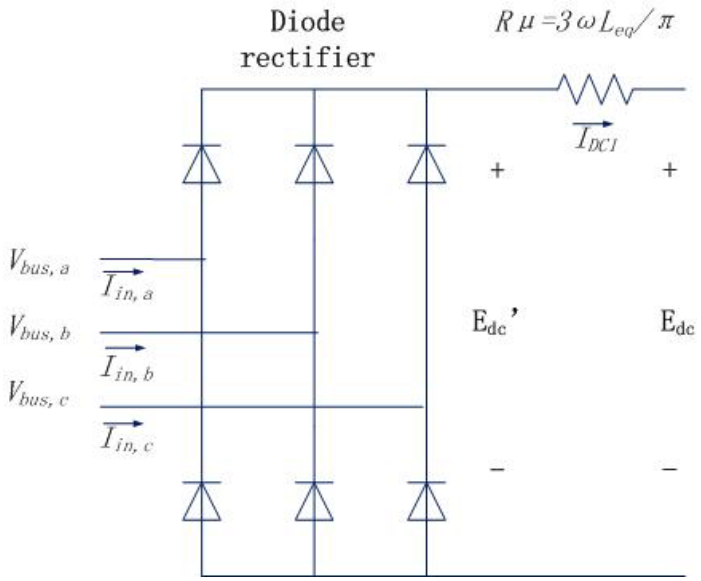

Figure 4. 3-phase diode rectifier with overlap angle resistance [11]

After introducing the equivalent variable resistance r_{μ}, we can simply consider the diode rectifier without concerning the effect of the overlap angle. The switching signal can be present as shown in Figure 5.

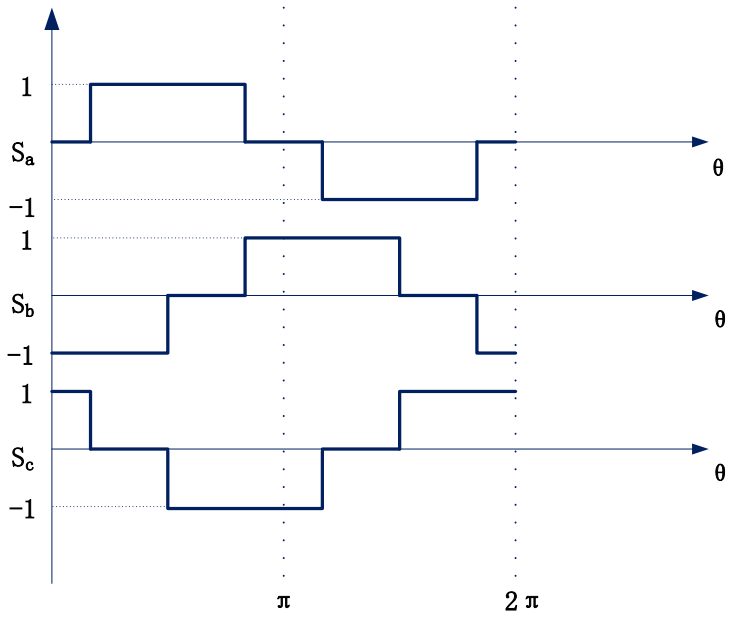

Figure 5. The rectifier switching signal

Assuming the output current of the rectifier is remain constant, then the input vectors from AC side can be expressed in terms of the switching function S_a and the DC side voltage and current as the following equations [18]:

$$\boldsymbol{I_{in,abc}} = \boldsymbol{S_{abc}} I_{DC1}$$

$$\boldsymbol{E'_{dc}} = \boldsymbol{S_a} V_{bus,a} + \boldsymbol{S_b} V_{bus,b} + \boldsymbol{S_c} V_{bus,c} \quad (2.\ 7)$$

So far we have the relationship between the input and output of the rectifier in the three-phase frame, the next work is to transfer the voltages and currents into the *d-q* reference frame.

For DQ method, we only consider about the fundamental component of the switching function [11]. The Fourier series of S_a as given in the following equation:

$$S_a = \sum_{k=1,5,7,\ldots}^{\infty} \frac{\sqrt{3}}{\pi} \cdot \frac{(-1)^{L+1}}{k} \cdot (-2 \sin k\omega t) \quad (2.\ 8)$$

If we consider the rectifier has a phase $\emptyset_b$, which lags the phase of the source voltage $\emptyset_s$ by an angle λ, then the fundamental component of S_a is calculated by setting k=1 in the above equation, as given in the following equations:

$$S_a = \frac{2\sqrt{3}}{\pi} \cdot (\sin \omega t - \emptyset_b)$$

$$S_b = \frac{2\sqrt{3}}{\pi} \cdot \left(\sin \omega t - \frac{2\pi}{3} - \emptyset_b\right)$$

$$S_c = \frac{2\sqrt{3}}{\pi} \cdot \left(\sin \omega t - \frac{4\pi}{3} - \emptyset_b\right) \quad (2.9)$$

The vector diagram below shows the phase relationship among the voltage source V_s, switching signal S and the input current I_{in}:

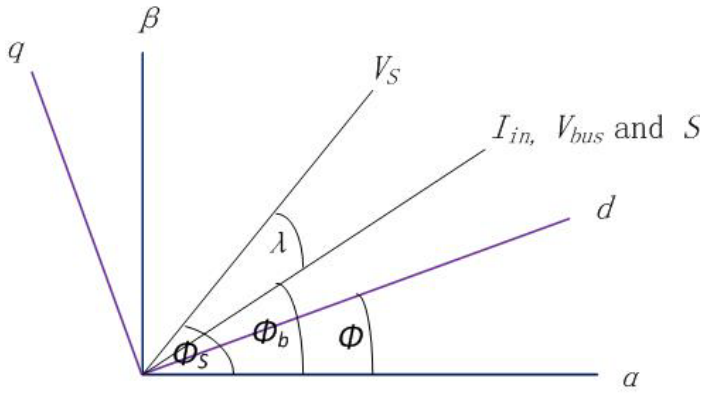

Figure 6. The vector diagram for DQ transformation

Notice that in the input current I_{in} is in phase with the input voltage $V_{bus.}$ Vs is the peak amplitude phase voltage of the source. S is the peak amplitude of switching signal. Now the vectors V_S, I_{in} and S can be presented into the DQ frame at rotating frequency $\omega t+\phi$ using the power conserving convention given in (2.10).

$$\boldsymbol{V_{S,dq}} = \sqrt{\frac{3}{2}} V_S e^{j(\phi_s - \phi)}$$

$$\boldsymbol{S_{dq}} = \sqrt{\frac{3}{2}} \left(\frac{2\sqrt{3}}{\pi}\right) e^{j(\phi_s - \phi)}$$

$$\boldsymbol{I_{in,dq}} = \sqrt{\frac{3}{2}} I_{in} e^{j(\phi_s - \phi)} \quad (2.10)$$

The equation above shows that the relationship between the peak amplitudes of currents and voltages from input terminal and output terminal can be calculated by (2.11).

$$\boldsymbol{I_{in,dq}} = \boldsymbol{S_{dq}} I_{DC1}$$

$$E_{DC}{}' = \boldsymbol{S_{dq}}^{\boldsymbol{T}} \boldsymbol{V_{dq}} \qquad (2.\ 11)$$

Which gives us a very interesting result — we can construct the rectifier into a transformer as shown in Figure 7.

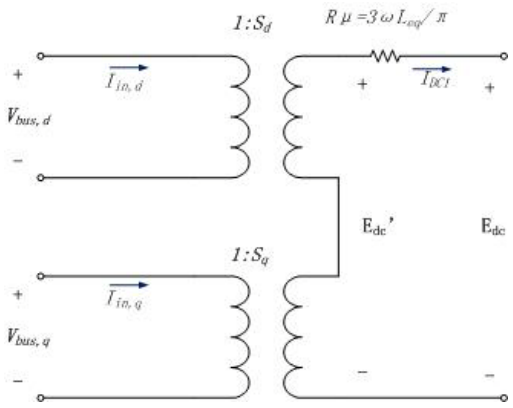

Figure 7. The equivalent circuit of rectifier in dq frame

The magnitude of the switching function S_d and S_q become the turn ratio of the transformers. The value of S_d and S_q are variant when the rotation reference frame changes.

If we only consider about the uncontrolled rectifier, by putting the other elements into the diode rectifier model, we obtain the equivalent circuit on *d*-*q* reference frame rotating at $\omega t+\phi$, as shown in Figure 8.

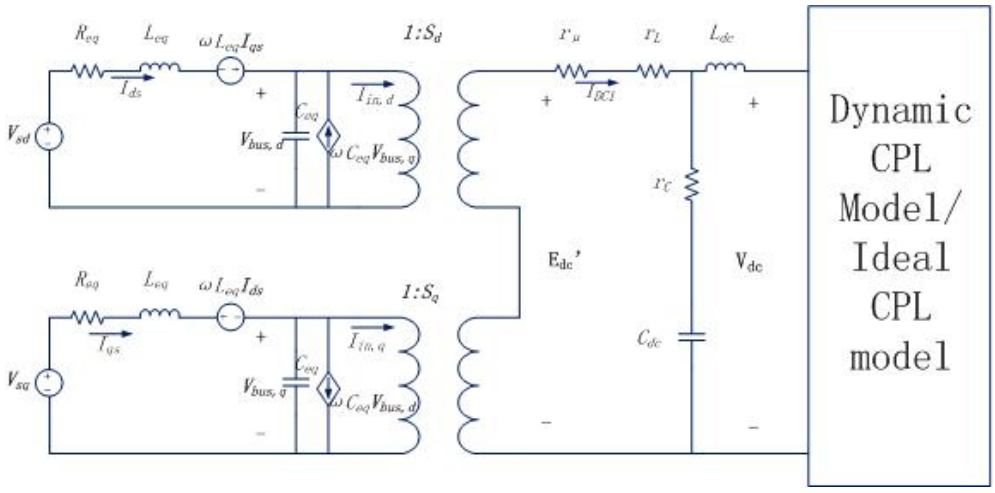

Figure 8. The equivalent circuit on *d-q* frame rotating at $\omega t+\phi$

Notice that the capacitor in the *d-q* reference frame can be viewed as a current source and the inductor is viewed as a voltage source depending on the system frequency.

This equivalent circuit can be simplified further. By fixing the rotating frame on the phase of the AC bus V_{bus}, the input terminal current in the *q*-axis, $I_{in,q}$, is equal to 0. Therefore the equivalent circuit given in Figure 8 can be simplified as shown in Figure 9.

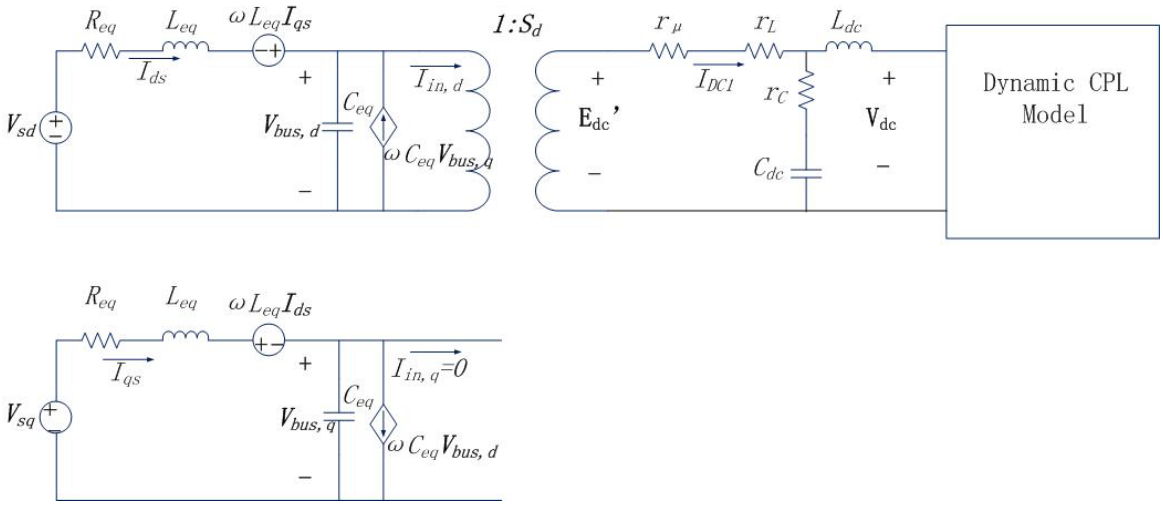

Figure 9. The simplified equivalent circuit of the power system

This simplified circuit will be used later, and is easier to analyse.

2.2.2 Controlled rectifier model

This section presents the modeling of the controlled rectifier part applying DQ transformation method. The analytical procedure of a controlled rectifier is very much like the procedure of the diode rectifier. The different between them is the switching function [19] and the double PI controller [20].

2.2.2.1 The equivalent circuit of controlled rectifier

By introducing an equivalent resistance r_μ located in the DC side as we did in the last section, we can simply apply the switching signal without considering the inductor effect. Assuming that the harmonics of the actual switching signal can be ignored, the switching function of the controlled rectifier is shown in Figure 10, in which α is the firing angle of thyristors.

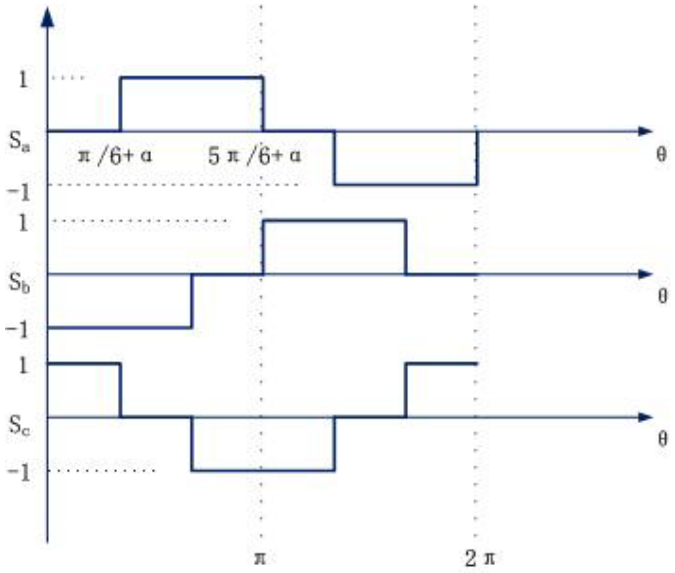

Figure 10. The switching signal of a controlled rectifier

Mathematically, the fundamental component of the switching function can be written as:

$$S_a = \frac{2\sqrt{3}}{\pi} \cdot (\sin \omega t + \emptyset - \alpha)$$

$$S_b = \frac{2\sqrt{3}}{\pi} \cdot \left(\sin \omega t - \frac{2\pi}{3} + \emptyset - \alpha\right)$$

$$S_c = \frac{2\sqrt{3}}{\pi} \cdot \left(\sin \omega t - \frac{4\pi}{3} + \emptyset - \alpha\right) \quad (2.\ 12)$$

in which $\emptyset$ is a phase angle of the AC bus. The vector diagram for the DQ transformation is shown in Figure 11.

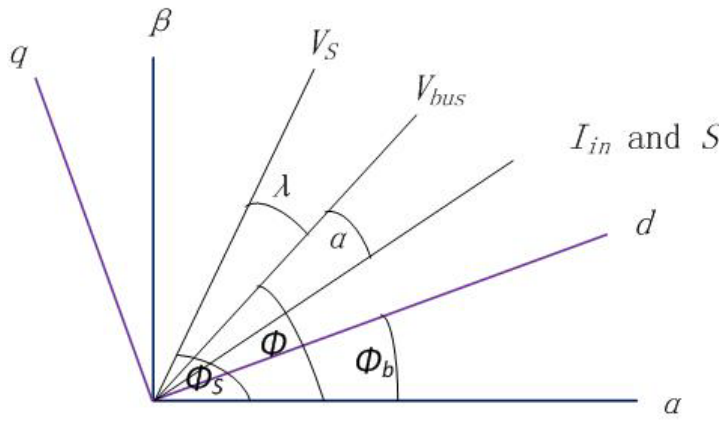

Figure 11. The vector diagram for DQ transformation

The relationship between input and output terminal of the controlled rectifier is as the same as the diode rectifier presented in the equation (2.10), (2.11). The switching function in the *d*-*q* reference frame is given by:

$$\mathbf{S_{dq2}} = \sqrt{\frac{3}{2}} \cdot \frac{2\sqrt{3}}{\pi} \begin{bmatrix} \cos(\phi_b - \phi + \alpha) \\ -\sin(\phi_b - \phi + \alpha) \end{bmatrix} \quad (2.\ 13)$$

The equivalent circuit of a controlled is the same as the model shown in Figure 7, except for the turn ratio of the transformer $\boldsymbol{S_{dq}}$. In a controlled rectifier, the firing angle α need to be taken into consideration. The equivalent circuit for a controlled rectifier and other elements without considering the uncontrolled diode rectifier subsystem can also be represented by Figure 8. The difference is in a controlled rectifier model, the *d*-*q* frame is rotating at $\omega t+\phi-\alpha$. This equivalent circuit can also be simplified to eliminate the transformer in the *q*-axis by align the vector of switching function *S* and the AC input current I_{in} with the *d*-axis. However, in order to get the

mathematic model for the whole system, we need to combine the two kinds of converters together, which require that both the diode rectifier and the thyristor rectifier select a same *d-q* reference frame. Then the model for the combination system of the two rectifiers can be presented as shown in Figure 12

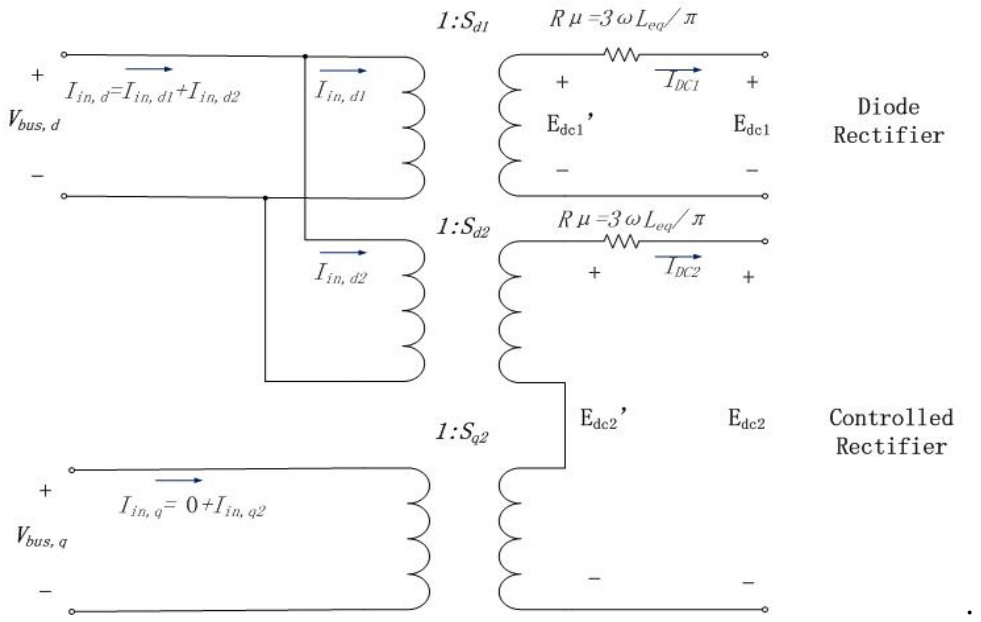

Figure 12. The combination system of the two rectifiers

From Figure 12 we can see that the total input current in *d-q* frame $I_{in,d}$ and $I_{in,q}$ are equal to the sum of the diode rectifier input terminal current and the controlled rectifier input terminal current in *d-q* frame correspondingly

2.2.2.2 Controllers of the system

This section presents the mathematic model for the controllers of the controlled rectifier system [20]. The subsystem studied is as shown in Figure 13.

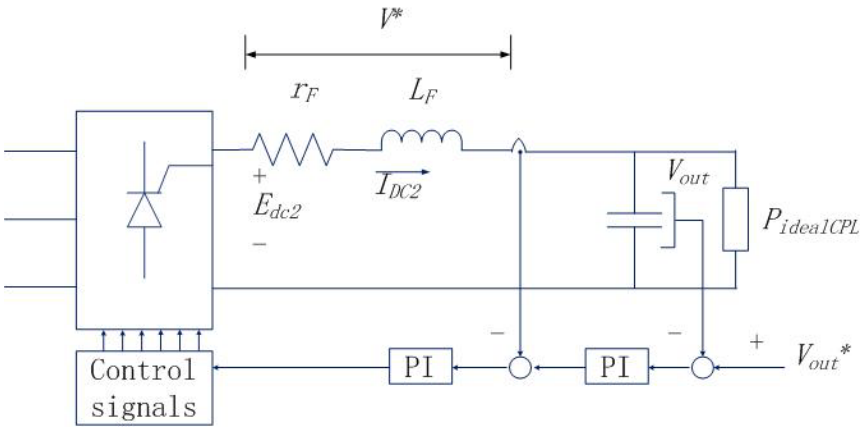

Figure 13. The considered system

The schematic of the controllers is as shown in Figure 14. It has two PI controllers cascaded, the first one regulates the output voltage of the converter, and the second one regulates the DC current.

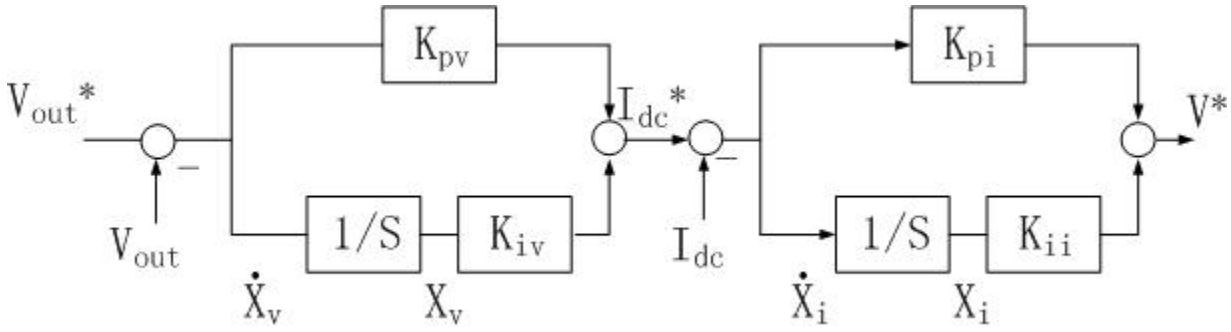

Figure 14. The schematic of the controllers

In Figure 14, V^* represents the reference voltage across the DC side resistor r_F and inductor L_F. This schematic contains two control loops: the inner loop is the current loop, and the outer loop is the voltage loop. Parameters I_{dc} and I_{dc}^* represents the actual and reference value of the current in DC side current, respectively. V_{out} and V_{out}^* represents the actual and reference value of the DC voltage, respectively. The parameters K_{pv} and K_{iv} are the proportional and integral gains of the voltage, and K_{pi} and K_{ii} are gains of the current. These gains of the PI controller can be

determined by classical method [19], or using ATS (Adaptive Tabu Search) and ABC (Artificial Bee Colony) method [21].

2.2.3 Electromechanical Actuator (EMA) models

In this section, the EMA model with controllers is illustrated. The first part gives the physical model of the motor and the second part provides the vector-controller of EMA.

2.2.3.1 Physical model of the PM machine

At the beginning, let us take a review on the principle of AC machine.

In an AC machine, assuming a three-phase balanced power supply in the three-phase stator winding, the magnetic field is rotating and sinusoidally distributed in the air gap [22]. If we give the definition for the following parameters:

P=number of poles of the machine;

ω_r=the rotor mechanical speed (r/s);

ω_e=the stator electrical speed (r/s);

$i_{a,b,c}$= phase currents in the three-phase stator winding;

I_m=the magnitude of the phase current;

N=number of turns in a phase winding;

Then $i_{a,b,c}$ are given as:

$$\begin{aligned} i_a &= I_m \cos\omega_e t \\ i_b &= I_m \cos\left(\omega_e t - \frac{2\pi}{3}\right) \\ i_c &= I_m \cos\left(\omega_e t + \frac{2\pi}{3}\right) \end{aligned} \tag{2. 14}$$

Each phase of currents results in a magnetomotive force (MMF). At a particular angle θ, the MMFs generated by phase currents are given in (2.15):

$$F_a(\theta) = Ni_a\cos\theta$$

$$F_b(\theta) = Ni_b\cos\left(\theta - \frac{2\pi}{3}\right)$$

$$F_c(\theta) = Ni_c\cos\left(\theta + \frac{2\pi}{3}\right) \quad (2.15)$$

Therefore, the total MMF at angle θ is given as:

$$\mathrm{F}(\theta) = F_a(\theta) + F_b(\theta) + F_c(\theta)$$

$$= Ni_a\cos\theta + Ni_b\cos\left(\theta - \frac{2\pi}{3}\right) + Ni_c\cos\left(\theta + \frac{2\pi}{3}\right) \quad (2.16)$$

Substitute (2.14) into (2.16) gives:

$$F(\theta,t) = NI_m[\cos\omega_e t\cos\theta + \cos\left(\omega_e t - \frac{2\pi}{3}\right)\cos\left(\theta - \frac{2\pi}{3}\right)$$

$$+ \cos\left(\omega_e t + \frac{2\pi}{3}\right)\cos\left(\theta + \frac{2\pi}{3}\right)] \quad (2.17)$$

Simplifying equation (2.17) results in:

$$F(\theta,t) = \frac{3}{2}NI_m\cos(\omega_e t - \theta) \quad (2.18)$$

This sweeping magnetic field subjects the rotation of the rotor.

In this study case, we use a PM machine as the driver. A PM synchronous machine uses a permanent magnet as the rotor instead of the dc field windings in the IM machine. It can be viewed as a special case of inductor drives. There are several advantages to apply a PM machine: to eliminate the field copper loss, has higher power density, has lower rotor inertia, and has more robust construction of the rotor. In general, although its cost is higher, a PM machine has higher efficiency than an IM machine.

To analyse the dynamic model of the PM drive, the DQ transformation is applying again. The steady-state analysis of PM machine is the same as a wound field machine except that the

equivalent field current should be considered as a constant, that is to say, the flux of the rotor F_m=constant. The equations in a rotating *d-q* reference frame getting from the PM machine's equivalent circuits using the peak convention, as given in the reference [22], are shown below:

$$V_{sqm} = R_{sm}I_{sqm} + \omega_e L_d I_{sdm} + \omega_e F_m + L_q \dot{I}_{sqm}$$

$$V_{sdm} = R_{sm}I_{sdm} - \omega_e L_q I_{sqm} + L_q \dot{I}_{sdm} \quad (2.\ 19)$$

This *d-q* reference frame is aligned with the rotor flux.

To simplify the analyzing process, two assumptions are made:

- Assuming the PM machine works in the full flux operation. This assumption results in I_{sdm}=0.
- Assuming constant flux generation and perfect field orientation during EMA operation. This assumption allows neglecting of I_{sdm} dynamic.

Therefore, the simplified equation shows the relationship between the input voltage V_{sm} and the input current I_{sm} can be written:

$$V_{sqm} = R_{sm}I_{sqm} + \omega_e F_m + L_q \dot{I}_{sqm}$$

$$V_{sdm} = -\omega_e L_q I_{sqm} \quad (2.\ 20)$$

In which the instantaneous speed ω_e is given by:

$$\omega_e = \frac{P}{2}\omega_r \quad (2.\ 21)$$

Applying Newton second law, the mechanical motion equation can be is given by [4]:

$$J_m \dot{\omega}_r = K_T I_{sqm} - T_L \quad (2.\ 22)$$

where J_m is the moment of inertia, T_L is the load torque and K_T is a constant defined as:

$$K_T = \frac{3}{2}\frac{P}{2}F_m \quad (2.\ 23)$$

Equation (2.20) through (2.23) presents above presented the physical model of the PM machine. Concluding these equations result into a block diagram as shown in Figure 15.

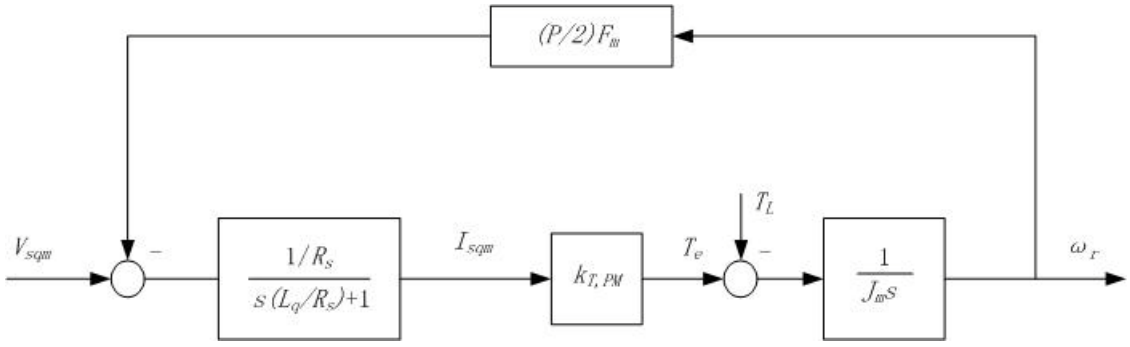

Figure 15. The model for the motor

In the next section, the controller of EMA will be introduced.

2.2.3.2 Controller of EMA

A standard motor drive vector-control structure applying double PI controllers is as shown in Figure 16[22]. There are two control loops: the inner loop is the current loop, which maintains the input terminal current of the PWM converter; the outer loop is the speed loop, which forces the rotation speed of the PM machine equal to the expected value. In this structure, the motor can be an IM motor (induction motor) or a PM motor (permanent magnet motor). For a PM machine operating at full flux operation, the model can be simplified by set I_{sdm} to zero.

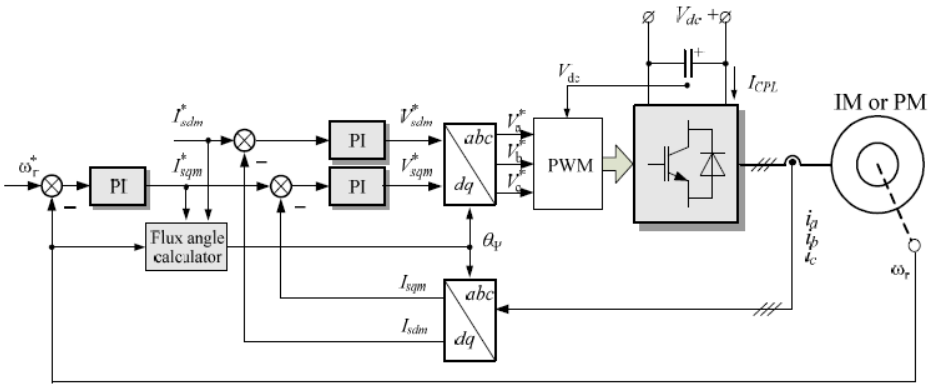

Figure 16. The standard motor drive control structure [4]

Without considering the d-axis current, the control structure can be simplified as only the q-axis current loop is analysed. The simplified control structure can be drawing as:

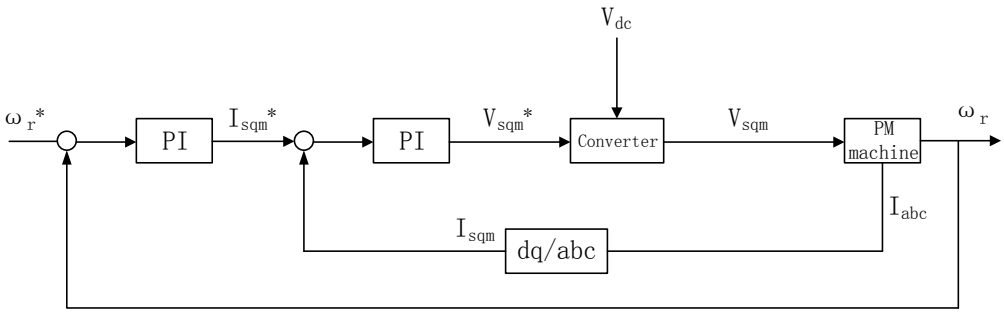

Figure 17. The control structure neglecting d-axis current dynamic

The two PI controllers in the

Figure 17 are defined as:

Speed controller: $k_{P\omega} + \frac{k_{I\omega}}{s}$, and q-axis current controller: $k_{Pi} + \frac{k_{Ii}}{s}$.

Then the following equations describing the speed and q-current dynamic PI controllers can be derived from the control structure:

$$k_{P\omega}k_{I\omega}^{-1}\dot{\omega}_r + k_{I\omega}^{-1}\dot{I}_{sqm}^* - k_{P\omega}k_{I\omega}^{-1}\dot{\omega}_r^* = -\omega_r + \omega_r^*$$

$$k_{PI}k_{Ii}^{-1}\dot{I}_{sqm} + k_{Ii}^{-1}\dot{V}_{sqm}^* - k_{Pi}k_{Ii}^{-1}\dot{I}_{sqm}^* = -I_{sqm} + I_{sqm}^* \quad (2.\ 24)$$

The controller output signal is the q-axis reference voltage $V_{sqm}{}^*$ feeding $V_{sqm}{}^*$ into the converter and through a PWM process result in the voltage V_{sqm}. This PWM process should be derived accurately in order to model the dynamic impact of DC-link voltage changes, especially on the DC link current. Figure 18 illustrates the non-linear block structure for the PWM process.

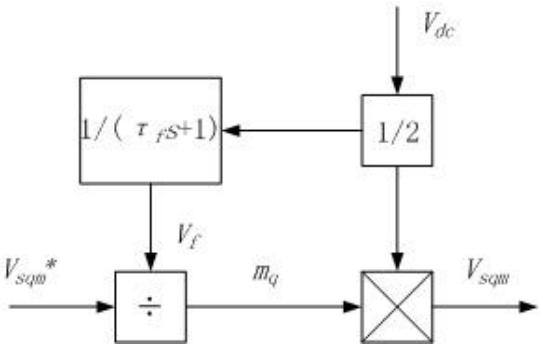

Figure 18. Modulation index calculator

The inverter output voltage V_{sqm} in the figure above is calculated using the filtered DC link voltage V_f. τ_f is the time constant of the filter, and m_q is the modulation indices. The mathematic relationship can be written as:

$$m_q = \frac{V_{sqm}^*}{V_f}$$

$$V_f = \frac{V_{dc}}{2} \cdot \frac{1}{1+s\tau_f} \qquad (2.\ 25)$$

The DC current of the inverter I_{CPL} can be calculated by applying the energy conservation conditions (assuming zero losses and setting I_{sdm}=0) as the following equation:

$$I_{CPL} = \frac{3}{2}\left[\frac{m_q I_{sqm}}{2}\right] \qquad (2.\ 26)$$

Now we have both physical model and control structure. Combining them together by summarizing equation (2.20) through (2.26) gives us the entire model of the controlled PM motor drive as a non-linear block diagram as shown in Figure 19.

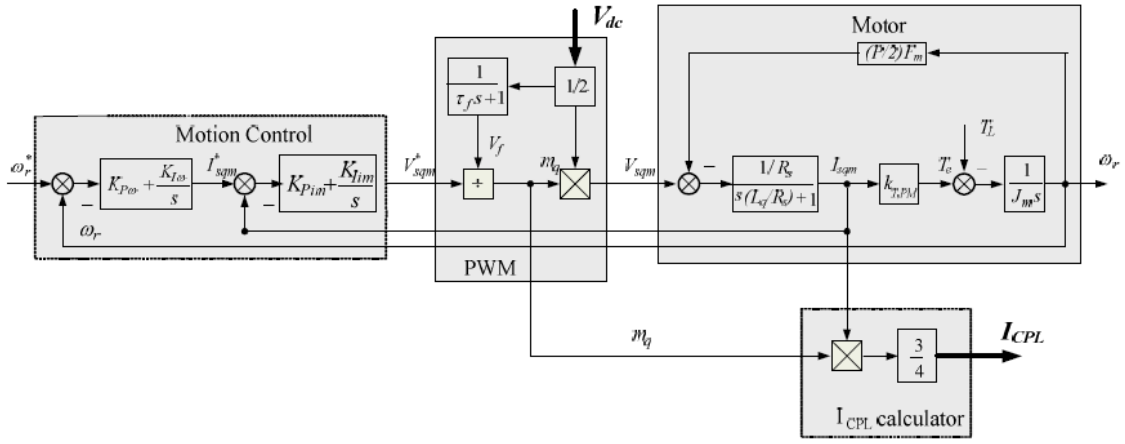

Figure 19. Block diagram of the non-linear EMA model for PM machine [4]

2.2.4 Ideal CPL load

When a motor is tightly controlled, it behaves as a constant power load. In other words, if the angular speed and the torque of the motor remain constant, the power of the motor will stay as a constant:

$$P = T \times \Omega = I \times V \tag{2. 27}$$

Let us consider about the following circuit:

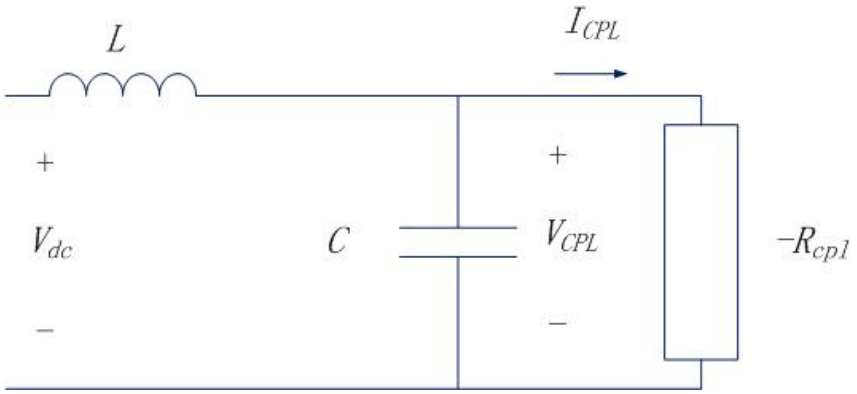

Figure 20. DC source feeding a CPL load through a low-pass filter

In Figure 20, due to the constant power, a small increment of current I_{CPL} will cause a small decrement of voltage V_{CPL}, and vise versa. Mathematically:

$$\frac{dV_{CPL}}{dI_{CPL}} < 0 = -R_{cpl} \tag{2. 28}$$

That is to say that a CPL causes a negative resistance.

A negative resistance will degrade the system stability. The dynamic model of Figure 20 can be written as:

$$V_{CPL} = \frac{V_{dc} \cdot \left(\frac{1}{sC} \parallel -R_{cpl}\right)}{sL + \frac{1}{sC} \parallel -R_{cpl}}$$

$$\frac{V_{CPL}}{V_{dc}} = \frac{R_{cpl}}{s^2 CLR_{cpl} - sL} \tag{2. 29}$$

It is clearly showing that the transfer function above has non-negative poles, which means the system could not be stable without a controller. The double PI controllers have already been introduced in the section 2.2.2.2, and they not only keep the output voltage equal to the reference, but also remain the DC current at a proper level.

An ideal CPL load can be modeled as a voltage-dependent current source:

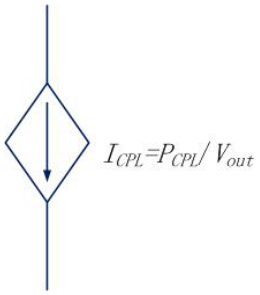

Figure 21. Ideal CPL load represented by a current source

In which V_{out} is the voltage across the DC-link capacitor and P_{CPL} is the power level of CPL.

2.2.5 Combined model of the whole studied system

So far we have analysed every part of the studied system in detail, now we can combine them together to get the mathematic model for the whole studied MEA power system.

2.2.5.1 Differential equations

For the converter part, considering the diode rectifier, the controlled rectifier with PI controller, the ideal CPL, and the AC side elements together, applying KVL and KCL on the circuit shown in Figure 8, we can write the following dynamic equations:

$$\dot{I}_{ds} = -\frac{R_{eq}}{L_{eq}} I_{ds} + \omega I_{qs} - \frac{1}{L_{eq}} V_{bus,d} + \frac{1}{L_{eq}} V_{sd}$$

$$\dot{I}_{qs} = -\omega I_{ds} - \frac{R_{eq}}{L_{eq}} I_{ds} - \frac{1}{L_{eq}} V_{bus,q} + \frac{1}{L_{eq}} V_{sq}$$

$$\dot{V}_{bus,d} = \frac{1}{C_{eq}} I_{ds} + \omega V_{bus,q} - \sqrt{\frac{3}{2}} \frac{2\sqrt{3}}{\pi C_{eq}} I_{dc1} - \sqrt{\frac{3}{2}} \frac{2\sqrt{3}}{\pi C_{eq}} cos\, \alpha\, I_{dc2}$$

$$\dot{V}_{bus,q} = -\omega V_{bus,d} + \frac{1}{C_{eq}} I_{qs} + \sqrt{\frac{3}{2}} \frac{2\sqrt{3}}{\pi C_{eq}} sin\, \alpha\, I_{dc2}$$

$$\dot{I}_{dc1} = -\frac{r_c C_{dc}}{L_{dc}} \dot{V}_{dc1} + \sqrt{\frac{3}{2}} \frac{2\sqrt{3}}{\pi L_{dc}} V_{bus,d} - \left(\frac{r_L}{L_{dc}} + \frac{r_\mu}{L_{dc}}\right) I_{dc1} - \frac{1}{L_{dc}} V_{dc1}$$

$$\dot{V}_{dc1} = \frac{1}{C_{dc}} I_{dc1} - \frac{1}{C_{dc}} I_{CPL1}$$

$$\dot{I}_{dc2} = -\left(\frac{r_F + K_{pi}}{L_F}\right) I_{dc} + \frac{K_{iv} K_{pi}}{L_F} X_v + \frac{K_{ii}}{L_F} X_i - \frac{K_{pv} K_{pi}}{L_F} V_{out2} + \frac{K_{pv} K_{pi}}{L_F} V^*_{out2}$$

$$\dot{V}_{out2} = \frac{1}{C_{dc}} I_{dc1} - \frac{1}{C_{dc}} \frac{P_{CPL2}}{V_{out2}}$$

$$\dot{X}_v = -V_{out} + V^*_{out}$$

$$\dot{X}_i = -I_{dc2} - K_{pv}V_{out} + K_{iv}X_v + K_{pv}V_{out}^* \tag{2. 30}$$

Note that both the equivalent circuit of diode rectifier and the controlled rectifier in the rotating *d-q* frame are fixed on the phase of V_{bus}. This makes the d-axis input current of the diode rectifier equals to $\sqrt{\frac{3}{2}}\frac{2\sqrt{3}}{\pi}I_{dc1}$, and *q*-axis input current equals to 0; and makes the d-axis input current of the controlled rectifier equals to $\sqrt{\frac{3}{2}}\frac{2\sqrt{3}}{\pi}\cos\alpha\, I_{dc2}$, and q-axis input current equals to $\sqrt{\frac{3}{2}}\frac{2\sqrt{3}}{\pi}\sin\alpha\, I_{dc2}$. Therefore the total input current in *d-q* frame $I_{in,d}$ and $I_{in,q}$ are equal to the sum of the diode rectifier input terminal current and controlled rectifier input terminal current in d-q frame correspondingly, as shown in the 3rd and 4th equation in (2.30). The last two equations of (2.30) describe the double PI control structure of the controlled rectifier in Figure 14. I_{CPL1} in the above equation corresponds to the DC current of EMA model calculated in (2.26), and P_{CPL2} corresponds to the power level of the ideal CPL load driving by the controlled rectifier.

For the EMA part, following equations summaries the dynamics of the PWM controlled PM motor:

$$J_m\dot{\omega}_r = K_T I_{sqm} - T_L$$

$$\dot{I}_{sqm} = -\frac{PF_m\omega_r}{2L_q} - \frac{R_{sm}}{L_q}I_{sqm} + \frac{V_{sqm}}{L_q}$$

$$\tau_f\dot{V}_f = -V_f + \frac{V_{dc}}{2}$$

$$\frac{K_{Pim}}{K_{Iim}}\dot{I}_{sqm} + \frac{\dot{V}_{sqm}^*}{K_{Iim}} - \frac{K_{Pim}\dot{I}_{sqm}^*}{K_{Iim}} = -I_{sqm} + I_{sqm}^*$$

$$\frac{K_{P\omega}}{K_{I\omega}}\dot{\omega}_r + \frac{\dot{I}_{sqm}^*}{K_{I\omega}} - \frac{K_{P\omega}\dot{\omega}_r^*}{K_{I\omega}} = -\omega_r + \omega_r^*$$

(2. 31)

The first three equations describe the physical model of EMA, which derived in section 2.2.3.1. The last two equations describe the vector controller of EMA, which derived in section 2.2.3.2.

2.2.5.2 Linearization and the state space model

For stability analysis, the set of equations (2.30)-(2.31) is linearized using the first order terms of the Taylor expansion. The general state space equations have the representation as the following matrix form:

$$\delta\dot{\mathbf{x}} = \mathbf{A}(x_0, u_0)\delta\mathbf{x} + \mathbf{B}(x_0, u_0)\delta\mathbf{u}$$
$$\delta\mathbf{y} = \mathbf{C}(x_0, u_0)\delta\mathbf{x} + \mathbf{D}(x_0, u_0)\delta\mathbf{u} \quad (2.32)$$

where the state variables are:

$$\mathbf{x} = [I_{ds}, I_{qs}, V_{bus,d}, V_{bus,q}, I_{dc1}, V_{dc1}, \omega_r, I_{sqm}, V_f, V^*_{sqm}, I^*_{sqm}, I_{dc2}, V_{out2}, X_v, X_i]^T \quad (2.33)$$

The matrix x has the dimension of 15×1.

The input matrix is written as:

$$\mathbf{u} = [\omega^*_r, T_L, V^*_{out2}]^T \quad (2.34)$$

The matrix u has the dimension of 3×1.

The output matrix is written as:

$$\mathbf{y} = [V_{dc1}, V_{out2}]^T \quad (2.35)$$

Which has the dimension of 2×1.

The detailed matrix A, B, C, and D are given in the appendix A.

3.0 SIMULATION AND RESULTS

In this chapter, the simulation applying MATLAB and the simulation results are presented. It is necessary to sort the fixed parameters at the beginning as shown in the appendix B. The result of applying the full state feedback controller is also presented in this chapter.

3.1 STABILITY ANALYSIS

In the simulation part, due to the difficulty of calculating the equilibrium point of the EMA model, it will only focus on the power levels of the EMA load rather than considering the parameter changes in the EMA model, and only consider about the DC output voltage of the controller rectifier. Now the system is simplified to a single input single output system.

The method for stability analysis in this chapter is using the eigenvalue theorem. The eigenvalue of the system can be calculated from the matrix $\mathbf{A(x_0,u_0)}$ in (2.32) by solving the eigenfunction:

$$\det[\lambda \mathbf{I}-\mathbf{A}]=0 \tag{3. 1}$$

The stability region of the system can be influenced by the system parameters. Table 2 shows the real part of the dominate eigenvalues of the system corresponding to different power levels.

Table 2. Real part of the system eigenvalues with different power levels

P_{EMA}(kW) / P_{CPL}(kW)	7	8	9	10
18	<0	<0	-1.9086×10^{2}	-1.925×10^{2}
19	<0	<0	-1.9087×10^{2}	2.31×10^{4}
20	<0	<0	-1.9088×10^{2}	2.394×10^{4}
21	<0	-1.8930×10^{2}	-1.9090×10^{2}	2.47×10^{4}
22	-3.0033×10^{2}	-1.8931×10^{2}	2.0717×10^{4}	2.5695×10^{4}
23	-3.0038×10^{2}	-1.8932×10^{2}	2.14×10^{4}	2.66×10^{4}
24	-3.0044×10^{2}	-1.8930×10^{2}	2.22×10^{4}	2.76×10^{4}
25	-1.878	1.8297×10^{4}	>0	>0
26	0.711×10^{2}	>0	>0	>0

From Table 2, we can easily get the stable and unstable region for varying the power level, as shown in Figure 22.

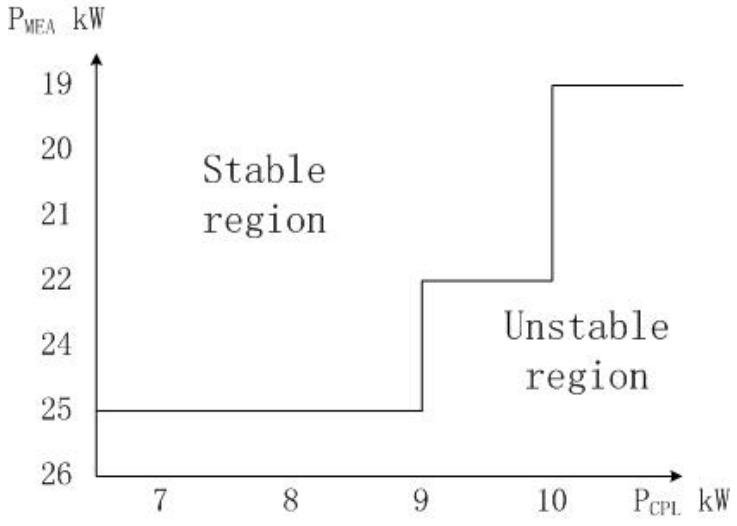

Figure 22. The stable and unstable region for varying the power level

A critical stable case at the point P_{EMA}=7kW, P_{CPL}=25kW has the step response as shown in Figure 23.

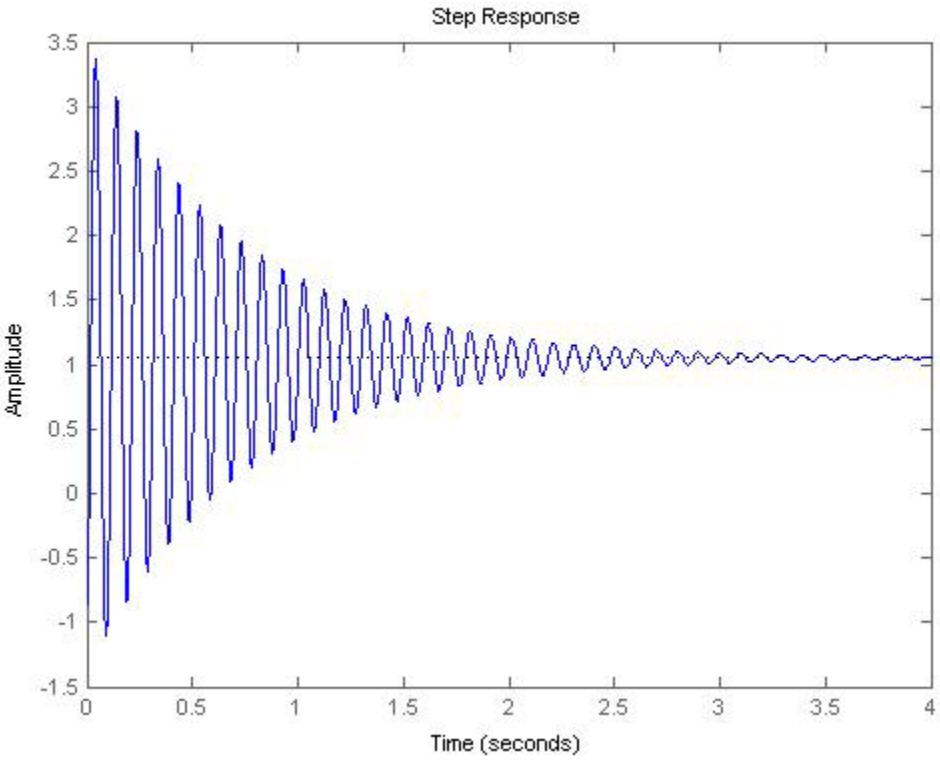

Figure 23. Step response of the system at (P_{EMA}=7kW, P_{CPL}=25kW)

An unstable case at the point P_{EMA}=6kW, P_{CPL}=26kW has the step response as shown in Figure 24.

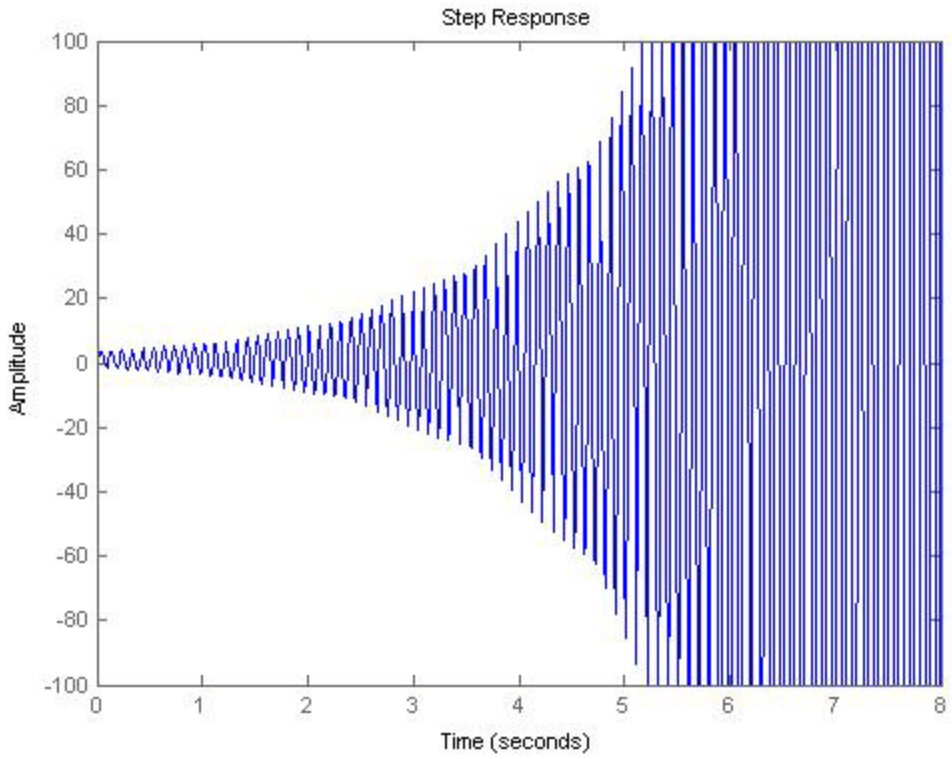

Figure 24. Step response of the system at (P_{EMA}=6kW, P_{CPL}=26kW)

From the stable region in the Figure 22, it can be seen that increasing CPL load can significantly degrade the system stability.

The frequency of the system can also influence the system stability region. Figure 25 shows the stability region of the system by fixing P_{CPL}=23000kW.

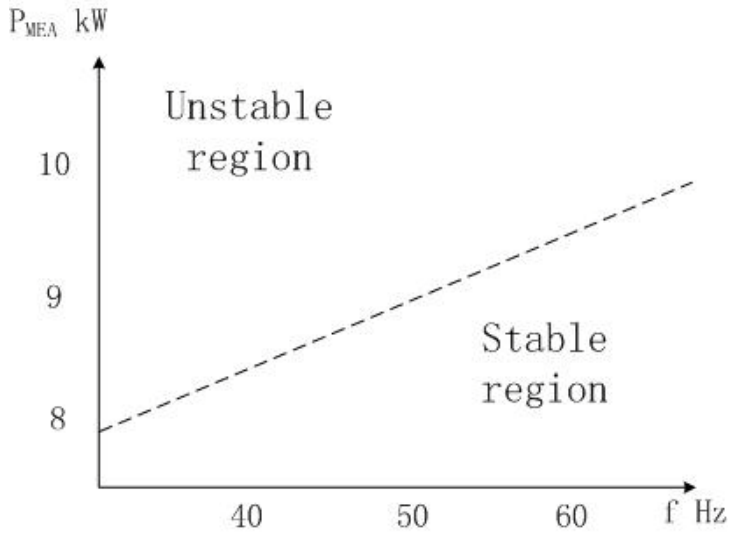

Figure 25. Instability line for changing frequencies

As we can see in the Figure 25, high system frequency upgrades the system stability.

3.2 APPLYING STATE FEEDBACK CONTROLLER

The theorem of the state feedback can be described as following [24]: If **(A, b)** is controllable, then by state feedback u=r-**kx**, the eigenvalues of **A-bk** can arbitrarily be assigned.

The principles for pole-placement and the procedures of **k** matrix calculation can be found in any modern control theory textbook, or we can get **k** using MATLAB function *place/acker*, therefore it is not necessary to put it in this thesis.

For the selection of feedback vector **k**, a classical method is to applying the linear quadratic regulator method. MATLAB offers a function to use this method and select the optimal coefficients **k** to stabilize the system.

Now let us design a state feedback controller for the case when P_{CPL}=10kW and P_{EMA}=50kW. The original system has the eigenvalues of 10014, $-373.37 \pm j9.1494 \times 10^7$, -

$375 \pm j9.1287 \times 10^7$, -27.5716, -303.81±j299.92, -23.6073±j58.4254, and we want to place all the poles to the left side of the s-plane.

The new system step response after the full-state feedback control is as shown in Figure 26.

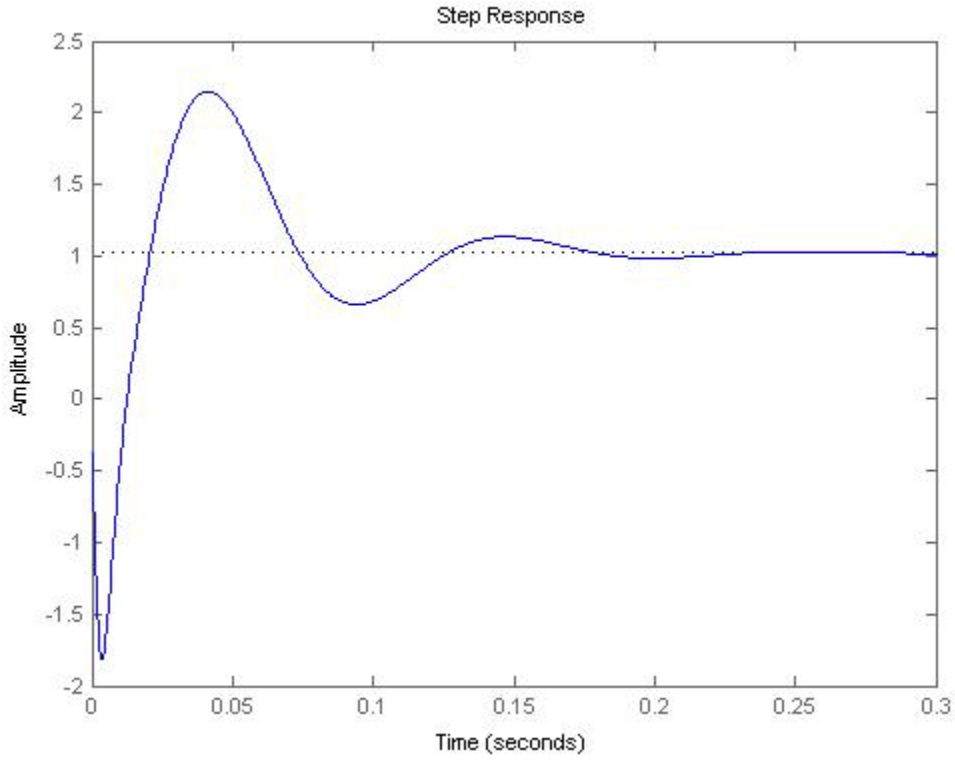

Figure 26. Step response after applying state feedback at P_{CPL}=10kW and P_{EMA}=50kW

From the figure above, we can see that the controlled system is stable but do not have good transient response. An adaptive control method presented in [21] can make a better result.

4.0 CONCLUSION

This thesis deals with the modeling and stability study of a MEA power system with hybrid converters and loads, and proposes a control design method using state feedback. DQ transformation method is used to derive the dynamic models of the diode rectifier and the controlled rectifier, and it is a convenient bridge to combine each subsystem. The EMA model is represented as a PM machine drive under the standard vector-control, however the equilibrium point is hard to evaluate and need a further study. An ideal CPL load degrades the system stability and modeled as a voltage-dependent current source. The results are validated by MATLAB, and the system stability region is analysed by calculating the system eigenvalues. To improve control performance, a full-state feedback control method is developed that can significantly increase the stability margin of MEA power system, however the transient response of the system is not as expected and more advanced control strategy need to be implemented as the future work.

APPENDIX A

THE DETAILS OF MATRICES OF THE STATE SPACE MODEL

The detail of matrix **A**:

$$\mathbf{A}(\mathbf{x_0}, \mathbf{u_0}) = \begin{bmatrix} \mathbf{A_M} & \mathbf{A_N} & \mathbf{A_O} \\ \mathbf{A_P} & \mathbf{A_Q} & 0 \\ 0 & 0 & \mathbf{A_R} \end{bmatrix}_{15\times15}$$

where

$$\mathbf{A_M} = \begin{bmatrix} -\frac{R_{eq}}{L_{eq}} & \omega & -\frac{1}{L_{eq}} & 0 & 0 & 0 \\ -\omega & -\frac{R_{eq}}{L_{eq}} & 0 & -\frac{1}{L_{eq}} & 0 & 0 \\ \frac{1}{C_{eq}} & 0 & 0 & \omega & -\sqrt{\frac{3}{2}}\frac{2\sqrt{3}}{\pi C_{eq}} & 0 \\ 0 & \frac{1}{C_{eq}} & -\omega & 0 & 0 & 0 \\ 0 & 0 & \sqrt{\frac{3}{2}}\frac{2\sqrt{3}}{\pi L_{dc}} & 0 & -\left(\frac{r_L + r_\mu + r_C}{L_{dc}}\right) & -\frac{1}{L_{dc}} \\ 0 & 0 & 0 & 0 & \frac{1}{C_{dc}} & 0 \end{bmatrix}_{6\times6}$$

$$\mathbf{A_N} = \begin{bmatrix} 0 & 0 & 0 & 0 & 0 \\ 0 & 0 & 0 & 0 & 0 \\ 0 & 0 & 0 & 0 & 0 \\ 0 & 0 & 0 & 0 & 0 \\ 0 & \frac{r_c C_{dc}}{L_{dc}} \frac{3M_{q0}}{4C_{dc}} & -\frac{r_c C_{dc}}{L_{dc}} \frac{3I_{sdm0} V_{sdm0}}{4C_{dc} V_{f,0}^2} & \frac{r_c C_{dc}}{L_{dc}} \frac{3I_{sqm0}}{4C_{dc} V_{f,0}} & 0 \\ 0 & -\frac{3M_{q0}}{4C_{dc}} & \frac{3I_{sdm0} V_{sdm0}}{4C_{dc} V_{f,0}^2} & -\frac{3I_{sqm0}}{4C_{dc} V_{f,0}} & 0 \end{bmatrix}_{6\times 5}$$

$$\mathbf{A_O} = \begin{bmatrix} 0 & 0 & 0 & 0 \\ 0 & 0 & 0 & 0 \\ -\sqrt{\frac{3}{2}} \frac{2\sqrt{3}}{\pi C_{eq}} \cos\alpha_0 & 0 & 0 & 0 \\ \sqrt{\frac{3}{2}} \frac{2\sqrt{3}}{\pi C_{eq}} \sin\alpha_0 & 0 & 0 & 0 \\ 0 & 0 & 0 & 0 \\ 0 & 0 & 0 & 0 \end{bmatrix}_{5\times 4}$$

$$\mathbf{A_p} = \begin{bmatrix} 0 & 0 & 0 & 0 & 0 & 0 \\ 0 & 0 & 0 & 0 & 0 & \frac{M_{q0}}{2\tau_s R_{sm}} \\ 0 & 0 & 0 & 0 & 0 & \frac{1}{2\tau_F} \\ 0 & 0 & 0 & 0 & 0 & -\frac{K_{pim} M_{q0}}{2\tau_s R_{sm}} \\ 0 & 0 & 0 & 0 & 0 & 0 \end{bmatrix}_{5\times 6}$$

$\mathbf{A_Q}$

$$= \begin{bmatrix} 0 & \frac{K_T}{J_m} & 0 & 0 & 0 \\ -\frac{PF_m}{2L_q} & -\frac{R_{sm}}{L_q} & -\frac{V_{sqm0}}{L_q V_{f,0}} & \frac{1}{L_q} & 0 \\ 0 & 0 & -\frac{1}{\tau_F} & 0 & 0 \\ -K_{pim}K_{l\omega} + \frac{PK_{pim}F_m}{2L_{eq}} & -K_{Iim} - \frac{K_{Pim}K_{p\omega}K_T}{J_m} + \frac{K_{Pim}R_{sm}}{L_q} & \frac{K_{Pim}V_{sqm0}}{L_q V_{f,0}} & -\frac{K_{Pim}}{L_q} & K_{Iim} \\ -K_{I\omega} & -\frac{K_{P\omega}K_T}{J_m} & 0 & 0 & 0 \end{bmatrix}_{5\times5}$$

$$\mathbf{A_R} = \begin{bmatrix} -\frac{(r_F + K_{pi})}{L_F} & -\frac{(K_{pv}K_{pi})}{L_F} & \frac{K_{iv}K_{pi}}{L_F} & \frac{K_{ii}}{L_F} \\ \frac{1}{C_F} & \frac{P_{CPL}}{C_F V_{out,0}^2} & 0 & 0 \\ 0 & -1 & 0 & 0 \\ -1 & -K_{pv} & K_{iv} & 0 \end{bmatrix}_{4\times4}$$

The details of matrix **B** (see next page):

$$\mathbf{B}(\mathbf{x_0}, \mathbf{u_0}) = \begin{bmatrix} 0 & 0 & 0 \\ 0 & 0 & 0 \\ 0 & 0 & 0 \\ 0 & 0 & 0 \\ 0 & 0 & 0 \\ 0 & 0 & 0 \\ 0 & -\frac{1}{J_m} & 0 \\ 0 & 0 & 0 \\ 0 & 0 & 0 \\ K_{PIm}K_{I\omega} & \frac{K_{PIm}K_{p\omega}}{J_m} & 0 \\ K_{I\omega} & \frac{K_{p\omega}}{J_m} & 0 \\ 0 & 0 & \frac{K_{Pv}K_{Pi}}{L_F} \\ 0 & 0 & 0 \\ 0 & 0 & 1 \\ 0 & 0 & K_{pv} \end{bmatrix}_{15\times 3}$$

The detail of matrix **C**:

$$\mathbf{C}(\mathbf{x_0}, \mathbf{u_0}) = [0 \quad 0 \quad 0 \quad 0 \quad 0 \quad 1 \quad 0 \quad 0 \quad 0 \quad 0 \quad 0 \quad 0 \quad 1 \quad 0 \quad 0]_{1\times 15}$$

The detail of matrix **D**:

$$\mathbf{D}(x_0, u_0) = [0 \quad 0 \quad 0]_{1\times 3}$$

APPENDIX B

SYSTEM PARAMETERS

Table 3. The system parameters

Parameters	Value
V_s	$230V_{rms/phase}$
ω	2π×50rad/s
R_{eq}	0.045Ω
L_{eq}	60μh
C_{eq}	2nF
rL	0.2Ω
L_{dc}	24.15mH
r_c	0.4Ω
C_{dc}	320μF
K_{pv}	0.101
K_{iv}	3.9478
K_{pi}	4.5442
K_{ii}	1257.4

BIBLIOGRAPHY

[1] J.A.Rosero, J.A. Ortega, E. Aldabas, and L. Romeral, "Moving Towards a More Electric Aircraft", *IEEE A&E Systems Magzine*, March 2007.

[2] A.Emadi, A. Khaligh, C. H. Rivetta, and G.A. Williamson, "Constant Power Loads and Negtive Impedance Instability in Automotive Systems: Definition, Modeling, Stability, and Control of Power Electronic Converters and Motor Drives," *IEEE Trans. On Vehicular Tech.*, vol. 55, no.4, pp. 1112-1125, July 2006.

[3] A. Emadi, B. Fahimi and M. Ehsani, "On the concept of Negtive Impedance Instability in the More Electric Aircraft Power Systems with Constant Power Loads," *Soc. Automotive Eng. J.*, pp.689-699, 1999

[4] Areerak, K-N, S.V. Bozhko, L. de Lillo, G.M. Asher, D.W.P. Thomas, A. Watson, T. Wu, "The Stability Analysis of AC-DC Systems Including Actuator Dynamics for Aircraft Power Systems," *In Proceedings of the 13th European Conference on Power Electronics and Applications, (EPE 2009)*, Barcelona, Spain, Sept. pp.8-10,2009

[5] J. Mahdavi, A. Emadi, M.D. Bellar and M. Ehsani, "Analysis of Power Electronic Converters Using the Generalized State-Space Averaging Approach," *IEEE Trans. On circuit and Systems*, vol. 44, pp.767-770, August 1997.

[6] Emadi, A., "Modeling and Analysis of Multi-converter DC Power Electronic Systems Using the Generalized State-space Averaging Method," *IEEE Trans. On Indus. Elect.*, vol. 51. No. 3, pp.661-668, June 2004.

[7] Emadi, A., "Modeling of Power Electronic Loads in AC Distribution Systems Using the generalized State-space Averaging Method," *IEEE Transactions on Indus. Elect.*, vol. 51. No. 5, pp.992-1000, Oct. 2004.

[8] Han, L., Wang, J. and Howe, D., "State-space Average Modeling of 6 and 12 pulse Diode Rectifiers," *In Proceedings of the 12th European Conference on Power Electronics and Applications*, Aalborg, Denmark, Sept. 2007

[9] Glover, S. F., "Modeling and Stability Analysis of Power Electronics Based Systems," Ph.D. dissertation, Purdue University, West Lafayette, IN, May 2003.

[10] Rim, C. T., Hu, D. Y., and Cho, G. H. "Transformers as Equivalent Circuits for Switches: General Proofs and DQ Transformation- based Analyses," *IEEE Transactions on Industry Applications*, vol. 26, No. 4, pp.777-785, July/Aug. 1990.

[11] Areerak, K-N, S.V. Bozhko, G.M.Asher, and D. W.P. Thomas, "Stability analysis and modeling of AC-DC System with Mixed Load Using DQ Transformation Method." *In Proceedings of the IEEE International Symposium on Industrial Electronics (ISIE08).*, Cambridge, UK, vol.29, pp.19-24, June-2/July 2008

[12] Areerak, K-N, S.V. Bozhko, G.M.Asher, L. De Lillo and D. W.P. Thomas, "Stability Study for a Hybrid AC-DC More-Electric Aircraft Power System", *IEEE Transactions on Aerospace and Electronic Systems*, vol.48, No.1 Jan. 2012

[13] "More Open Electrical Technologies European FP6 Project: http://www.moetproject.eu.

[14] T.Wu, S. Bozhko, G.Asher, P. Wheeler, and D. Thomas, "Fast Reduced Functional Models of Eletromechanical Actuators for More-Electric Aircraft Power System Study", *SAE International Conference 2008*, Seattle, USA, November 2008.

[15] Kundur P. "Power system stability and control [M]". New York: McGraw-hill, 1994.

[16] Temesgen Mulugeta Haileselassie, "Control of Multi-terminal VSC-HVDC Systems", Master of Science in Energy and Environment, Department of Electrical Power Engineering, Norwegian University of Science and Technology, Trondheim, 2008.

[17] N.Mohan, T.M. Underland, and W.P. Robbins, *Power Electronics: Converters, Applications, and Design*, John Wiley & son, USA, 2003, pp. 106-108.

[18] M. Sakui, H. Fujita, and M. Shioya, "A Method for Calculating Harmonic Currents of a Three-Phase Bridge Uncontrolled Rectifier with DC Filter," IEEE Trans. On Indus. Elect., vol. 36, no.3 pp. 434-440, August 1989.

[19] Koson Chaijaroenudomrung, Kongpan Areeak, Kongpol Areeak, "The Stability Study of AC-DC Power System with Controlled Rectifier Including Effect of Voltage Control", *European Journal of Scientific Research*, ISSN 1450-216X Vol.62 No.4 (2011), pp. 463-480, EuroJorunals Publishing, Inc. 2011

[20] Chaijaroenudomrung, K., K-N., Areerak, and K-L., Areerak, 2010. "Modeling of Three-phase Controlled Rectifier using a DQ method", *2010 International Conference on Advances in Energy Engineering (ICAEE 2010)*, Beijing, China: June 19-20, pp.56-59.

[21] Koson Chaijarurnudomrung, Kongpan Areerak, Kongpol Areerak, and Umaporn Kwannetr, "Optimal Controller Design of Three-Phase Controlled Rectifier Using Artificial Intelligence Techniques", *ECTI Transactions on Electrical Eng., Electronics, and Communications*, Vol. 10, No.1 Feb. 2012

[22] B. K. Bose: Modern Power Electronics and AC Drives, Prentice Hall, 2002

[23] K-N Areerak, S. V. Bozhko, G.M. Asher, and D. W. P. Thomas, "DQ-Transformation Approach for Modelling and Stability Analysis of AC-DC Power System with Controlled PWM Rectifier and Constant Power Loads" In *Proceedings of the 13 th International Power Electronics and Motion Control Conference* (EPE-PEMC 2008), pp.2070-2077 Poznan, Poland, Sept. 1-3, 2008,.

[24] C.-T. Chen. Linear System Theory and Design, 3rd Edition, Oxford University Press, 1999.